



Article

Influence of Chemical Weathering and Microcracks on Permeability Variations in Crystalline Rocks

Jinyoung Park ¹, Seongwoo Jeong ², Seonggan Jang ², Juyeon Lee ², Kyoungtae Ko ^{3,*} and Minjune Yang ^{1,4,*}¹ Wible Co., Ltd., Busan 48548, Republic of Korea; jypark@wible.kr² Major of Earth and Environmental Sciences, Division of Earth Environmental System Sciences, Pukyong National University, 45 Yongso-ro, Nam-gu, Busan 48513, Republic of Korea; seongwoo@pukyong.ac.kr (S.J.); seonggan@pukyong.ac.kr (S.J.); juyeon_lee@pukyong.ac.kr (J.L.)³ Geology Division, Geological Research Center, Korea Institute of Geoscience and Mineral Resources, Daejeon 34132, Republic of Korea⁴ Major of Environmental Geosciences, Division of Earth Environmental System Sciences, Pukyong National University, 45 Yongso-ro, Nam-gu, Busan 48513, Republic of Korea

* Correspondence: kkt@kigam.re.kr (K.K.); minjune@pknu.ac.kr (M.Y.)

Abstract: Rock permeability, an important factor in subsurface fluid migration, can be influenced by microcracks and chemical weathering due to water–rock interactions. Understanding the relationship between permeability, chemical weathering, and microcracks is crucial for assessing fluid flow in rocks. This study focuses on the hydrogeological characteristics of granite and gneiss, potential host rocks for high-level radioactive waste disposal in South Korea. Samples were analyzed for permeability, porosity, P-wave velocity, and chemical weathering indices. Regression analysis revealed a weak correlation between permeability and both porosity and rock density, while an inverse correlation was observed between permeability and chemical weathering indices. Interestingly, some samples showed low permeability (10^{-21} to 10^{-22} m²) despite high weathering, while others showed high permeability (10^{-18} to 10^{-19} m²) despite low weathering. SEM-EDS analysis indicated the presence of microcracks within the rocks or the filling of these cracks with secondary minerals. The findings suggest that chemical weathering generally increases pore size and porosity, but actual permeability can vary depending on the presence and connectivity of microcracks and the extent to which they are filled with secondary minerals. Therefore, both chemical weathering and microcrack connectivity must be considered when evaluating the hydrogeological characteristics of crystalline rocks.

Keywords: chemical weathering; chemical weathering index; porosity; permeability; P-wave velocity; crystalline rock



Citation: Park, J.; Jeong, S.; Jang, S.; Lee, J.; Ko, K.; Yang, M. Influence of Chemical Weathering and Microcracks on Permeability Variations in Crystalline Rocks. *Water* **2024**, *16*, 3007. <https://doi.org/10.3390/w16203007>

Academic Editor: Yu Huang

Received: 11 September 2024

Revised: 17 October 2024

Accepted: 19 October 2024

Published: 21 October 2024



Copyright: © 2024 by the authors. Licensee MDPI, Basel, Switzerland. This article is an open access article distributed under the terms and conditions of the Creative Commons Attribution (CC BY) license (<https://creativecommons.org/licenses/by/4.0/>).

1. Introduction

Rock permeability is a crucial hydrogeological property that significantly influences fluid migration in subsurface environments [1]. It assumes particular importance in isolation repositories for substances like high-level radioactive waste (HLRW) disposal facilities and CO₂ geological storage sites, which rely on subsurface geological characteristics [2–4]. In HLRW disposal facilities, impermeable rocks serve as host formations in the underlying strata to effectively impede the migration of radioactive elements [2,5,6]. Granite, metamorphic rocks, and shale are commonly used as host rocks because of their low permeability [7–11]. Similarly, in CO₂ geological storage sites, the caprock functions in a manner analogous to the host formation in radioactive waste facilities, acting as a barrier to prevent the upward leakage of stored CO₂, thus necessitating low permeability [12,13]. Consequently, permeability is a critically important characteristic of barrier-forming rocks, emphasizing the need to investigate the permeability properties of rock formations comprising the target layer during site selection for disposal facilities.

The permeability of deep aquifer rocks can undergo significant changes due to the presence of microcracks generated by physical impacts such as earthquakes and chemical weathering resulting from water–rock interactions [14]. Chemical weathering from these reactions can dissolve primary minerals or precipitate secondary minerals, thereby altering rock porosity and subsequently affecting permeability [15]. Under conditions dominated by water–rock reactions, chemical weathering can increase both the porosity and permeability of initially low-permeability rocks. Even in the absence of chemical weathering, microcracks within the rock can act as conduits for fluid movement, leading to a substantial increase in permeability [16–18]. Therefore, to assess the fluid flow characteristics of rocks, it is crucial to consider the interplay between permeability, the degree of chemical weathering, and the presence of microcracks.

Chemical weathering alters the chemical composition of rock through dissolution and precipitation processes resulting from water–rock reactions. Rock dissolution reactions vary depending on mineral solubility; as chemical weathering progresses, minerals that are more easily dissolved experience a decrease in their constituent elements, whereas minerals with relatively higher resistance to dissolution show an increase in their constituent element ratios. Furthermore, precipitation reactions can increase the constituent elements of the precipitated minerals. Changes in rock chemical composition due to dissolution and precipitation have been utilized in various fields to estimate the degree of chemical weathering, often employing chemical weathering indices. Generally, in rocks undergoing chemical weathering, the concentrations of alkali elements, alkaline earth metals, and silica tend to decrease due to their higher mobility, whereas elements such as Al, Fe, Mn, and Ti tend to increase or remain relatively constant [19,20]. For example, plagioclase, which constitutes a significant portion of the minerals in granite, has a relatively high solubility compared with other minerals. Therefore, the preferential dissolution of plagioclase during chemical weathering leads to a decrease in Na, Ca, K, and SiO₂ elemental concentrations while increasing the relative Al₂O₃ proportion, which is a less mobile element within the rock.

Chemical weathering indices have been used to indicate the degree of weathering in crystalline rocks, such as granite and gneiss [21–26]. Weathering can also significantly decrease rock strength, and some studies have explored the relationship between chemical weathering indices and rock mechanical properties [16,17,23,27–30]. For instance, Liu et al. [29] investigated the effects of chemical weathering on granite's mechanical properties, finding that it significantly reduces strength and stability, increasing erosion susceptibility. They highlighted the importance of using chemical weathering indices to quantify weathering, as these indices correlate strongly with changes in the rock's structural characteristics. In another study, Kubo et al. [16] examined the influence of microcracks on the permeability and hydrogeological properties of granitic rocks. They observed that chemical weathering not only increased the overall porosity but also promoted the development of microcracks, further enhancing the rock permeability. The presence of these microcracks provided additional pathways for fluid movement, significantly impacting the hydrogeological characteristics of the rock. Sausse et al. [30] focused on microcrack porosity and fluid permeability in granites, finding that chemical weathering-induced microcracks play a crucial role in increasing permeability by creating interconnected pore networks. They concluded that chemical weathering processes lead to the development of microcracks and increased porosity, which in turn enhances the permeability of granite. These studies suggest that chemical weathering plays a critical role in enhancing the permeability of crystalline rocks by increasing porosity and developing microcracks. However, while the increase in permeability due to chemical weathering has been extensively reported, the potential decrease in permeability resulting from precipitation reactions during chemical weathering has received much less attention. Therefore, research on the impact of secondary mineral precipitation due to chemical weathering on the hydrogeological properties of crystalline rocks is lacking.

The overall objective of this study is to provide foundational data on the impact of chemical weathering and the distribution of microcracks on fluid flow in crystalline bedrock,

particularly for applications such as HLRW disposal site selection. To achieve this, the specific objectives were to (1) investigate the hydrogeological characteristics of granite and gneiss in the study areas; (2) analyze the chemical compositions of the samples to identify chemical weathering conditions that might contribute to increased permeability; (3) assess the relationships between crystalline rock permeability, porosity, P-wave velocity (V_p), and the degree of chemical weathering; and (4) identify microcrack distributions on sample matrix surfaces to provide insight into the contribution of microcracks to permeability.

2. Study Area and Rock Samples

Figure 1 shows the drilling locations and geological maps of the granite and gneiss used in this study. Two deep boreholes were drilled in Daejeon (granite) and Andong (gneiss) and entirely cored to a depth of approximately 1 km to investigate the hydrogeological, geophysical, geochemical, mineralogical, and stratigraphical characteristics (Figure 1). The Daejeon region belongs to the Okcheon Belt, based on the Korean Peninsula tectonic structure, and is located on the Mesozoic Daebong granite bedrock [31]. Mesozoic Jurassic two-mica granite is widely distributed throughout the study area. Two-mica granite has medium-to-fine crystal sizes and consists mainly of quartz, alkali feldspar, plagioclase, and biotite [32]. The Andong region is located at the Gyeongsang Basin boundary and contains mainly Paleoproterozoic gneiss. The study area has prevalent alkaline gneiss composed mainly of hornblende, biotite, and feldspar. The gneiss is heterogeneous due to a mixture of foliation and blocky structures and is characterized by various crystal sizes [31]. In total, 21 granite samples and 15 gneiss samples were collected at various depths from the drill cores for use in this study. Both rock samples were used to measure permeability, porosity, weathering degree, and V_p .

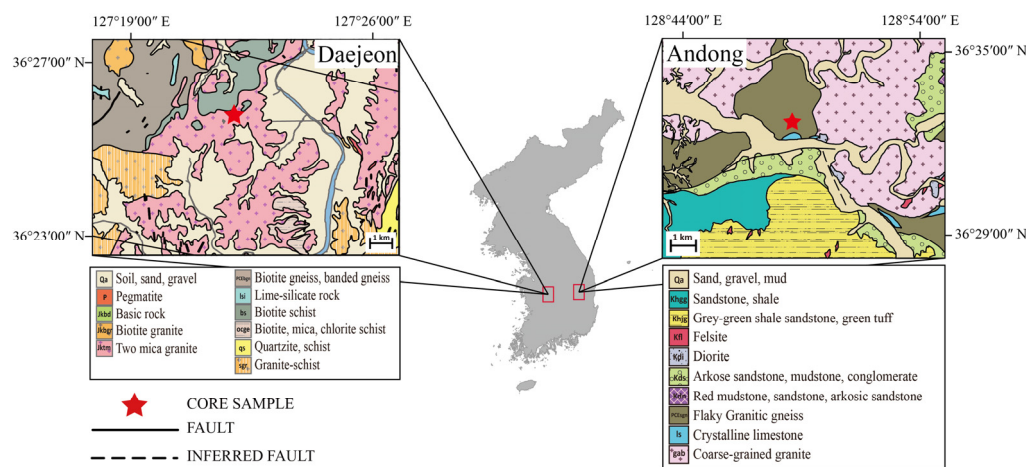


Figure 1. Geological map of boreholes with two rock types (granite and gneiss) used in this study. Granite and gneiss samples were collected at Daejeon and Andong, respectively.

3. Measurement and Analysis Methods

3.1. Hydrogeological Characteristics

3.1.1. Permeability

Core flooding experiments were conducted to estimate the permeability of the drill core samples. These experiments simulate in situ fluid flow conditions more realistically by replicating subsurface environments where fluids pass through the core sample under controlled pressures. Considering the high-pressure cell specifications, all samples were approximately 50 mm in diameter and manufactured with a length of 60–70 mm. The schematics of the permeability measurement equipment used in this study are shown in Figure 2a. Nitrogen gas, an inert gas with almost no chemical reaction with other substances, was used as the injection fluid for the permeability measurements [8]. The high-pressure core holder used in the experiment had a pressure resistance of 380 bar and consisted of

a cylindrical rubber sleeve to fix the drill core sample inside the holder. The rock sample was placed in the sleeve, and a confining pressure was applied by injecting water with a hand pump (ENERPAC P141, Menomonee Falls, WI, USA). The confining pressure was set at 20–30 bar higher than the injection pressure, and end pieces were mounted at both ends of the rock sample. Nitrogen gas was injected through the inlet using a syringe pump (TELEDYNE ISCO 500HP, Louisville, KY, USA), and the nitrogen gas flux passing through the rock sample was measured in real-time using a mass flow meter (MFM) (BROOKS 5860E, PA, USA). The nitrogen gas injection pressure was set in stages to measure the flux in the steady flow state for each pressure. The gas permeability (k_{act}) at steady flow was calculated using the following equation [33]:

$$k_{act} = \frac{2000p_a\mu q_a L}{(P_1^2 - P_2^2)A} \quad (1)$$

where p_a is the atmospheric pressure (atm), μ is the gas viscosity (cP), q_a is the gas flow rate measured at atmospheric pressure (cm^3/s), L is the core sample length (cm), P_1 is the inlet pressure (atm), P_2 is the outlet pressure (atm), and A is the rock sample cross-sectional area (cm^2). The outlet pressure was considered equal to the atmospheric pressure (1 atm).

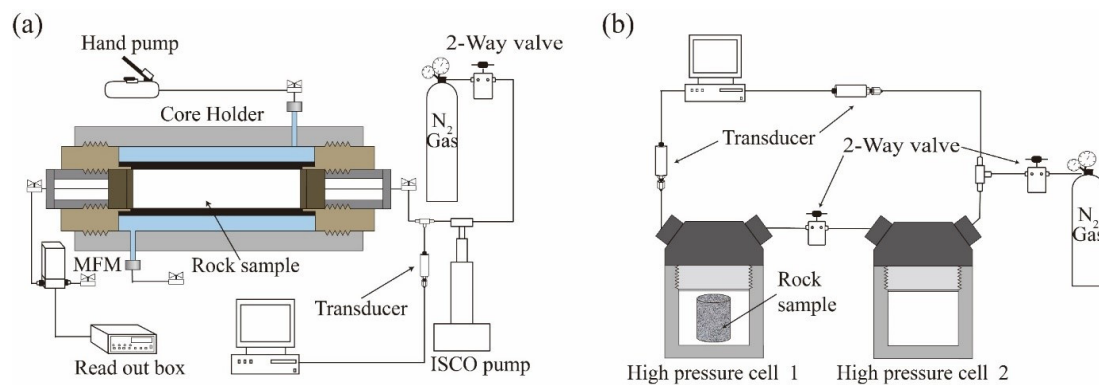


Figure 2. The schematics of the apparatus used to measure (a) permeability and (b) porosity in this study.

The permeability measured using gas as the injection fluid was calculated differently based on the pressure conditions due to the Klinkenberg effect, which results from gas molecule slippage along the pore surface at low flow rates [34]. Therefore, the Klinkenberg calibration is particularly important for low-permeability rocks, as it is necessary to obtain a permeability equivalent to the actual permeability under deep geological conditions [34]:

$$k_a = k_{act} \left(1 + \frac{\beta}{P_m} \right) \quad (2)$$

where k_a is the actual permeability corrected by the Klinkenberg calibration, β is the Klinkenberg slippage factor, and P_m is the mean pressure between the inlet and outlet.

In this study, five points of k_{act} were considered when increasing the injection pressure per sample to 30 bar to estimate k_a . As previously mentioned, the maximum permissible pressure of the permeability measurement instrument used in this study was 380 bar. The gas mass flow detection limit in the MFM was 5 mL/min. To obtain five points of k_{act} per sample, 5 mL/min of gas flux must be detected at a pressure of at least 300 bar. From Equation (1), a minimum k_{act} of $9.6 \times 10^{-21} \text{ m}^2$ was determined, and the minimum value of k_a that can be obtained using Equation (2) is $4.0 \times 10^{-22} \text{ m}^2$. The permeability measurement was repeated three times, and the average value was used as the result.

3.1.2. Porosity

The equipment used for the porosity measurement consisted of two chambers: one for the sample measurement and one as a reference. A schematic diagram of the porosity measurement setup is shown in Figure 2b. The advantage of this method is that it allows the same rock sample used for permeability measurements to be utilized for porosity measurements without any deformation. This enables a clearer evaluation of the correlation between porosity and permeability using the same rock sample. Porosity measurements were conducted using the same core samples as the permeability measurements to identify the correlation between porosity, permeability, and V_p . The porosity measurement method is based on Boyle's law, in which the pressure of a gas is inversely proportional to its volume at a constant temperature:

$$P_1(V_1 - V_g) + P_2V_2 = P_e(V_1 + V_2 - V_g) \quad (3)$$

The dried core sample was placed in a measurement chamber with a volume of V_1 , nitrogen gas was injected to apply a pressure of P_1 . Nitrogen gas was injected into a reference chamber with a volume of V_2 and pressure of P_2 . The valve connecting the two chambers was then opened, and the pressure at equilibrium was recorded. These recorded pressures were substituted into Equation (3) to determine the volume of the dried core sample. The volume (V_g) of each dried sample was calculated using Equation (3).

The rock sample porosity was determined using the following equation:

$$\varnothing = \frac{V_b - V_g}{V_b} \quad (4)$$

where \varnothing is the porosity and V_b is the bulk volume of the rock sample. Porosity measurements were also performed in triplicate, and the arithmetic mean of these measurements was used as the final porosity value.

3.2. P-Wave Velocity

As minerals dissolve during the chemical weathering process, the increase in pore size and number leads to a decrease in rock density. Therefore, some previous studies have compared the degree of chemical weathering by analyzing differences in P-wave velocity based on changes in rock density [4,16–18]. P-wave velocity (V_p) was measured using the direct transmission method to assess the correlation between V_p and permeability. To measure the V_p , a Pundit PL-200 (Proceq instrument, Schwerzenbach, Swiss), two 54 kHz transducers (pulse, receive), standard couplant gel, and a calibration rod were used. A schematic diagram of the V_p measurement is shown in Figure 3. A Pundit device and calibration rod were used to ensure signal reading accuracy. The V_p was obtained by placing two transducers on opposite sides of the core sample. The V_p test mechanism comprised a pulse transducer that propagated the P-wave through the core sample and a receiver transducer that received the P-wave. The travel time and distance traveled by the transmitted wave were used to compute the V_p . The two core sample surfaces were polished to flatten them, and a couplant gel was used to closely attach the transducer to the core surface. When the P-wave velocity reached a steady state, the P-wave data were recorded using the measuring instrument.

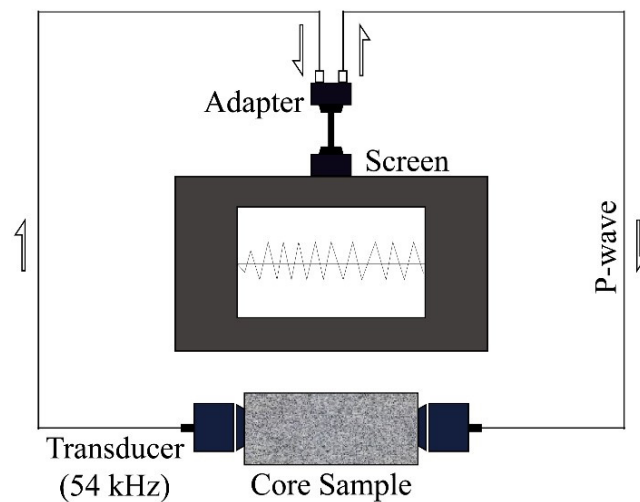


Figure 3. The schematics of the apparatus used to measure V_p in this study.

3.3. Chemical Weathering Indices

To quantitatively assess the chemical weathering of granite and gneiss, four chemical weathering indices were calculated using the chemical compositions obtained by X-ray fluorescence (XRF) analysis (Shimadzu MXF-2400, Kyoto, Japan). XRF was used because of its high accuracy in quantifying elemental concentrations, particularly for key elements such as Si, Al, and Fe, which are important for assessing the degree of chemical weathering. During chemical weathering, differences in the mobility of elements cause changes in their ratios within the rock. In this study, we aimed to evaluate the degree of chemical weathering by using chemical weathering indices developed based on these elemental mobility differences. The selection of these specific indices, including the Ruxton ratio (RR), sesquioxide content (SOC), chemical weathering index (CWI), and product index (PI), was based on their relevance and sensitivity to various aspects of chemical weathering processes (Table 1).

The RR is calculated as the ratio of SiO_2 , which is mobile during weathering, to Al_2O_3 , which is relatively immobile. A lower RR value indicates a higher intensity of weathering [35,36]. Rocks with RR values over 10 are considered fresh, while values close to 0 indicate significant weathering. This index effectively distinguishes between unweathered and highly weathered samples by reflecting the differential mobility of silica and alumina during weathering processes.

The SOC is an index reflecting the Fe_2O_3 content through iron oxidation and the Al_2O_3 content, which is resistant to weathering. SOC values increase as weathering progresses, making it a valuable indicator of the extent of chemical weathering [37]. This index was selected because it directly measures the accumulation of weathering-resistant oxides, providing insight into the progressive stages of weathering.

The CWI represents the ratio of chemical constituents related to the total chemical content affected by weathering. This index closely correlates with the physical properties of weathered granite [38]. For fresh rock, CWI values range from 15 to 20, while weathered rock values range from 20 to 40. The CWI was chosen due to its comprehensive reflection of the overall chemical alteration in the rock, capturing a broad spectrum of weathering processes.

The PI measures the content of immobile elemental oxides. Its value decreases as weathering intensity increases, with the highest values found in debris and residual soil and the lowest in partly weathered rocks [39,40]. This index was included because it quantifies the accumulation of stable weathering products, providing a direct measure of the degree of chemical weathering.

Table 1. Chemical weathering indices used in this study.

Chemical Weathering Index	Formula	Reference
Ruxton ratio (RR)	$\text{SiO}_2/\text{Al}_2\text{O}_3$	[36]
Chemical weathering index (CWI)	$100 \times (\text{Al}_2\text{O}_3 + \text{Fe}_2\text{O}_3 + \text{TiO}_2 + \text{H}_2\text{O}) /$ all chemical components	[38]
Sesquioxide content (SOC)	$\text{Al}_2\text{O}_3 + \text{Fe}_2\text{O}_3$	[37]
Weathering product index (PI)	$100 \times [\text{SiO}_2 / (\text{SiO}_2 + \text{TiO}_2 + \text{Fe}_2\text{O}_3 + \text{Al}_2\text{O}_3)]$	[40]

3.4. Correlation Analysis

In order to examine the correlations between the variables (weathering indices, permeability, porosity, etc.) employed in this study, Pearson correlation analysis (r) was conducted. The Pearson correlation coefficient is expressed as follows:

$$r = \frac{\sum_{i=1}^N (x_i - \bar{x})(y_i - \bar{y})}{\left[\sum_{i=1}^N (x_i - \bar{x})^2 \right] \left[\sum_{i=1}^N (y_i - \bar{y})^2 \right]} \quad (5)$$

where x and y represent the variables under investigation, and \bar{x} and \bar{y} are the mean values of these variables. The numerator in Equation (5) represents the covariance between the two variables, while the denominator signifies the product of the standard deviations of the two variables. This standardized measure of correlation evaluates the linear relationship between the variables, with values ranging from -1 to 1 , indicating perfect negative and positive correlations, respectively.

Furthermore, to assess the statistical significance of the Pearson correlation coefficients, a two-tailed t -test was performed, with the significance level set at 0.05 . According to the conventional criteria for hypothesis testing, if the significance probability (p -value) exceeds 0.05 , the null hypothesis is retained, suggesting that there is no statistically significant correlation between the variables. Conversely, if the p -value is less than 0.05 , the null hypothesis is rejected in favor of the alternative hypothesis, which posits a significant correlation between the variables. A p -value below 0.05 thus indicates that the correlation between the two factors is statistically significant, confirming a reliable association within the dataset.

3.5. Rock Matrix and Microcrack Distribution

The presence of microcracks in rock significantly contributes to increased permeability by reducing tortuosity [3]. The extent of microcrack development and connectivity can have a substantial impact on the hydraulic properties of the rock, regardless of the degree of chemical weathering. To examine the microcracks and mineralogical characteristics of the rock samples, scanning electron microscopy with energy-dispersive spectroscopy (SEM-EDS) (JEOL JSM-7610F, Tokyo, Japan) was used at the Center for Research Facilities at Gyeongsang National University. SEM-EDS analysis was conducted using thin sections that were infiltrated and solidified with resin to preserve the original crack shapes and prevent the generation of secondary cracks during sample preparation. These thin sections were prepared to identify the effects of differences in mineral structure and the presence of microcracks on permeability. The prepared thin sections were examined using SEM to observe the structure of the constituent minerals, the presence of microcracks, and the connectivity of these microcracks. EDS was used to analyze the elemental composition of the minerals within the rock and the secondary minerals filling the microcracks.

4. Results and Discussion

4.1. Correlation Between Porosity and Permeability

The distributions of porosity and permeability with depth for granite and gneiss samples are shown in Figure 4. The porosity of the granite samples was below 1.0% , aver-

aging around 0.5%, with permeability ranging from $7.9 \times 10^{-19} \text{ m}^2$ to $1.4 \times 10^{-21} \text{ m}^2$, except for three samples that were lower than the measurement limit ($<4.0 \times 10^{-22} \text{ m}^2$) (Figure 4a). The gneiss samples showed an average porosity of approximately 0.4%, and permeability varied from $3.6 \times 10^{-18} \text{ m}^2$ to $4.6 \times 10^{-22} \text{ m}^2$ (Figure 4b). Typically, granite and gneiss show porosity values ranging from 0.1% to 1.5% and permeability values from 10^{-21} m^2 to 10^{-16} m^2 [10,41–43]. However, the measured values in this study were generally similar to or lower than these typical ranges. Notably, the measured values for both rock types demonstrated an increasing trend with depth. Generally, porosity is expected to decrease with depth due to mechanical compaction under high-pressure conditions underground [44]. Nevertheless, in this study, the porosity of the rocks in the lower parts was higher than in the upper parts, suggesting that the lower samples were more altered and weathered, leading to increased voids and cracks. Some gneiss core samples, in particular, displayed high permeability (approximately $3.0 \times 10^{-18} \text{ m}^2$), indicating the presence of numerous microcracks in those sections.

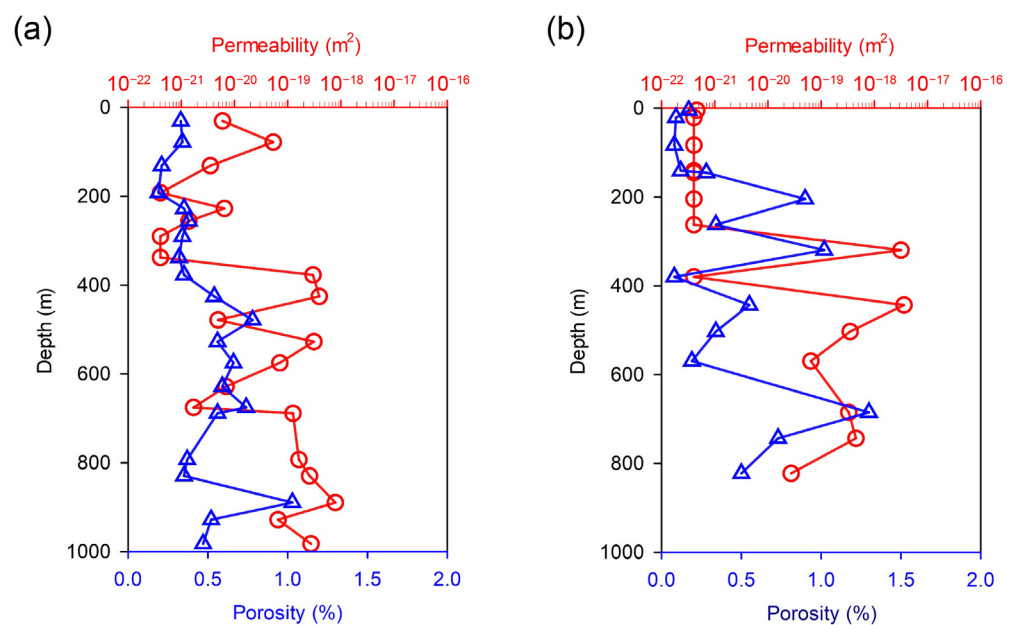


Figure 4. Permeability and porosity measurement results for (a) granite and (b) gneiss samples based on sample depth. Red lines and circles represent permeability values, while blue lines and triangles represent porosity values.

Figure 5 shows positive correlations between porosity and permeability for both granite and gneiss, suggesting that rocks with higher porosity tend to have higher permeability. The correlation coefficients between porosity and permeability for both rock types indicate moderate correlations (granite: $r = 0.52$, $p < 0.05$ and gneiss: $r = 0.41$, $p < 0.05$). This moderate correlation is due to certain granite samples showing high permeability regardless of porosity. Specifically, samples from depths of 375 to 425 m and 690 to 980 m showed high permeability (about 10^{-18} to 10^{-19} m^2) despite having similar porosity to other granite samples. For gneiss, samples from depths of 400 to 600 m showed relatively high permeability despite having low porosity. These variations in permeability, despite similar porosity levels, might be attributed to the presence and distribution of microcracks, which likely developed in these sections and significantly contributed to the increased permeability [16].

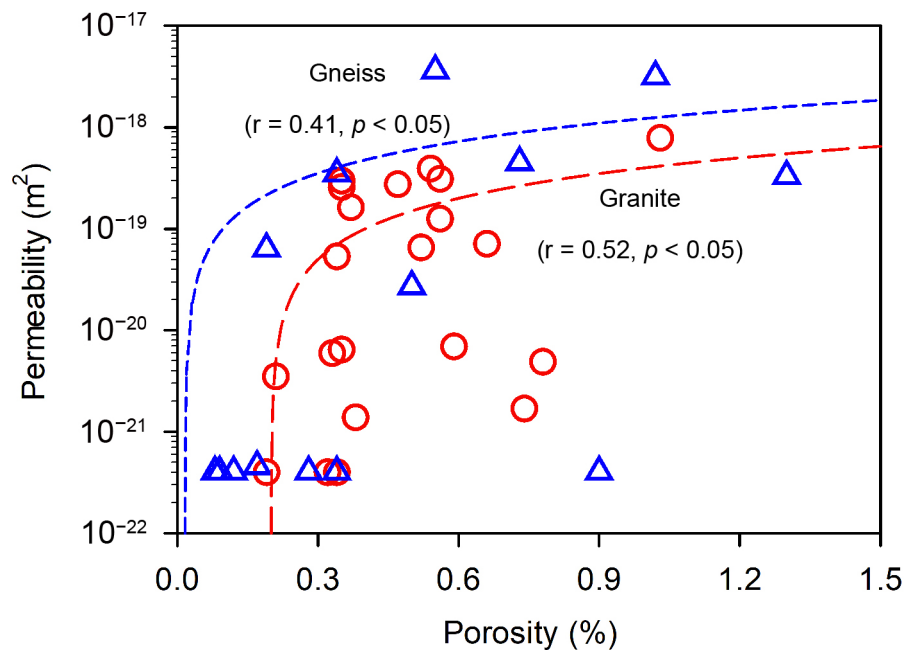


Figure 5. Correlations between permeability and porosity of both rock types. Red circles represent granite sample correlated values, while blue triangles represent gneiss sample correlated values. The long (red) and short (blue) dashed lines indicate the correlation between the porosity and permeability of granite and gneiss, respectively.

4.2. Correlation Between P-Wave Velocity and Permeability

The correlation between V_p and permeability for the granite and gneiss samples is shown in Figure 6. The V_p of the granite samples ranged from 2821 to 5156 m/s, while that of the gneiss samples ranged from 3687 to 6471 m/s. A strong negative correlation was observed between permeability and V_p for granite ($r = -0.8, p < 0.05$), and a weak negative correlation for gneiss ($r = -0.32, p < 0.05$). Generally, higher V_p values correspond to denser rock structures with fewer pores and lower permeability, as well-cemented structures reduce porosity and the number of interconnected pores, limiting groundwater flow [45–47]. However, a lower V_p does not always correlate with higher permeability. Some gneiss samples showed relatively low permeability despite their low V_p , suggesting that secondary minerals such as carbonate and clay may block groundwater movement by filling pores or microcracks.

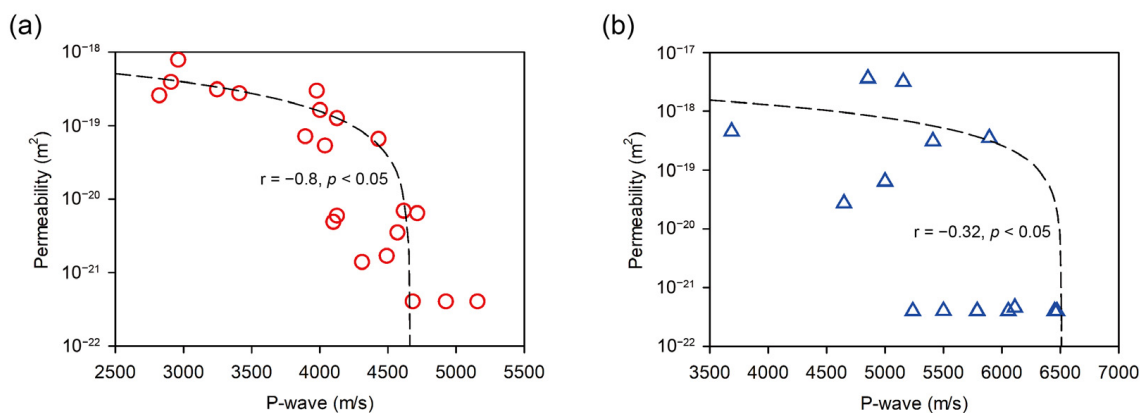


Figure 6. Correlations between permeability and V_p for (a) granite and (b) gneiss samples.

4.3. Correlation Between Chemical Weathering Indices and Permeability

The correlation between the Si and Al contents in the granite and gneiss samples is shown in Figure 7. The Si and Al contents showed a very strong or strong negative correlation (granite: $r = -0.97$, $p < 0.05$ and gneiss: $r = -0.77$, $p < 0.05$). This negative correlation is explained by the difference in mobility between Si and Al during chemical weathering. The Si/Al ratio represents the degree of chemical weathering [36]. As chemical weathering progresses, Si is leached out by the dissolution of silicate minerals, while Al remains in precipitated clay minerals as a by-product of silicate mineral dissolution [16,37]. In this study, granite and gneiss samples with a relatively low Si content and high Al content (low Si/Al ratio) indicate that they have undergone more chemical weathering than other samples. Furthermore, the chemical weathering likely occurred more extensively in rocks with relatively higher permeability.

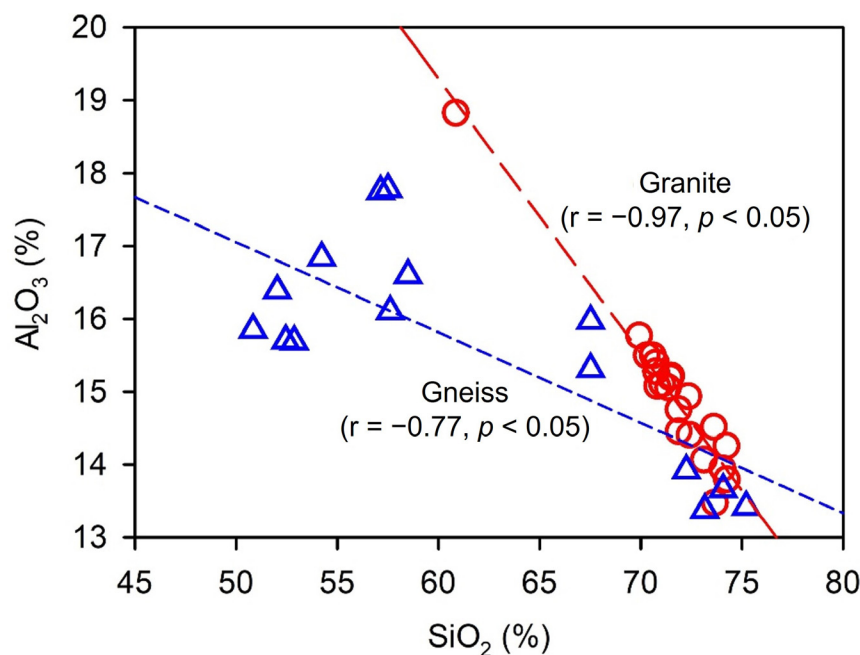


Figure 7. Correlation between Al_2O_3 and SiO_2 content of both rock types. Red circles represent granite sample correlated values, while blue triangles represent gneiss sample correlated values. The long (red) and short (blue) dashed lines indicate the correlation between the porosity and permeability of granite and gneiss, respectively.

The correlation between chemical weathering indices and permeability for granite and gneiss is shown in Figures 8 and 9. Granite samples showed weak correlations between permeability and the chemical weathering indices (RR: $r = 0.36$, $p < 0.05$; CWI: $r = -0.40$, $p < 0.05$; SOC: $r = -0.33$, $p < 0.05$; PI: $r = 0.33$, $p < 0.05$), while gneiss showed relatively moderate correlations (RR: $r = 0.60$, $p < 0.05$; CWI: $r = -0.60$, $p < 0.05$; SOC: $r = -0.58$, $p < 0.05$; PI: $r = 0.56$, $p < 0.05$). Lower values for RR and PI indicate increased chemical weathering, whereas higher values for CWI and SOC represent more advanced weathering. Based on these indices, it is typically expected that rocks with higher degrees of weathering would show lower permeability. However, in this study, samples with higher weathering indices showed lower permeability, contrary to previous findings.

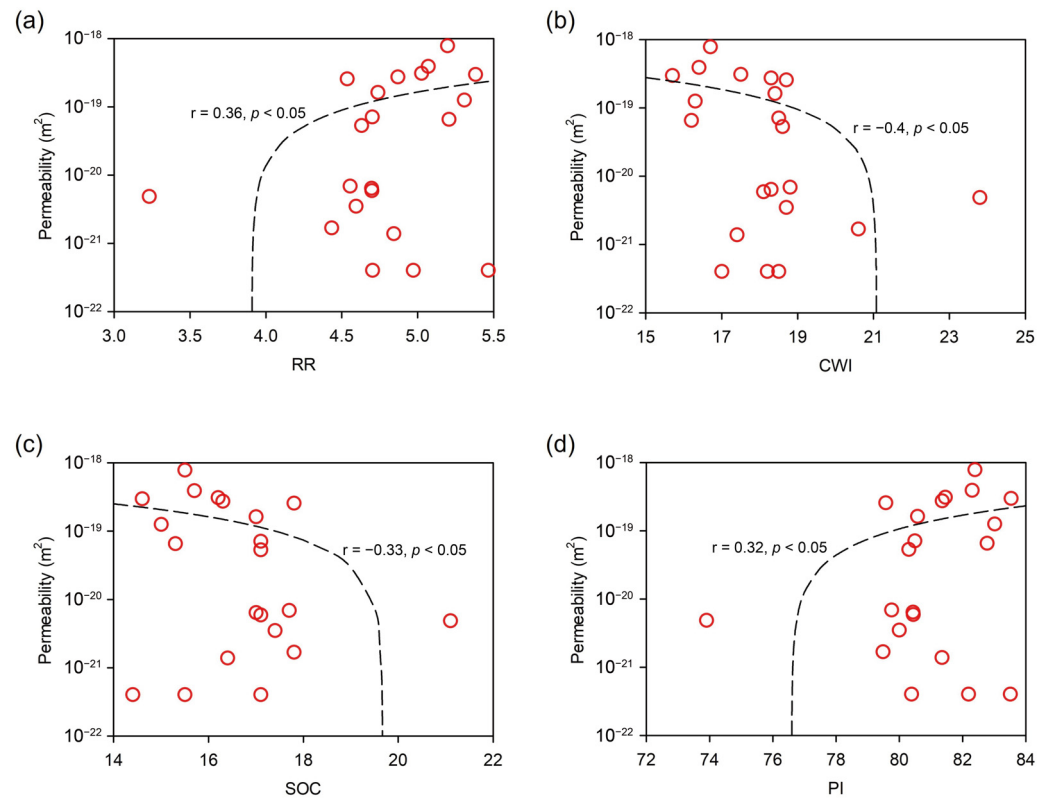


Figure 8. Correlation between permeability and chemical weathering indices ((a) RR; (b) CWI; (c) SOC; (d) PI) for granite samples.

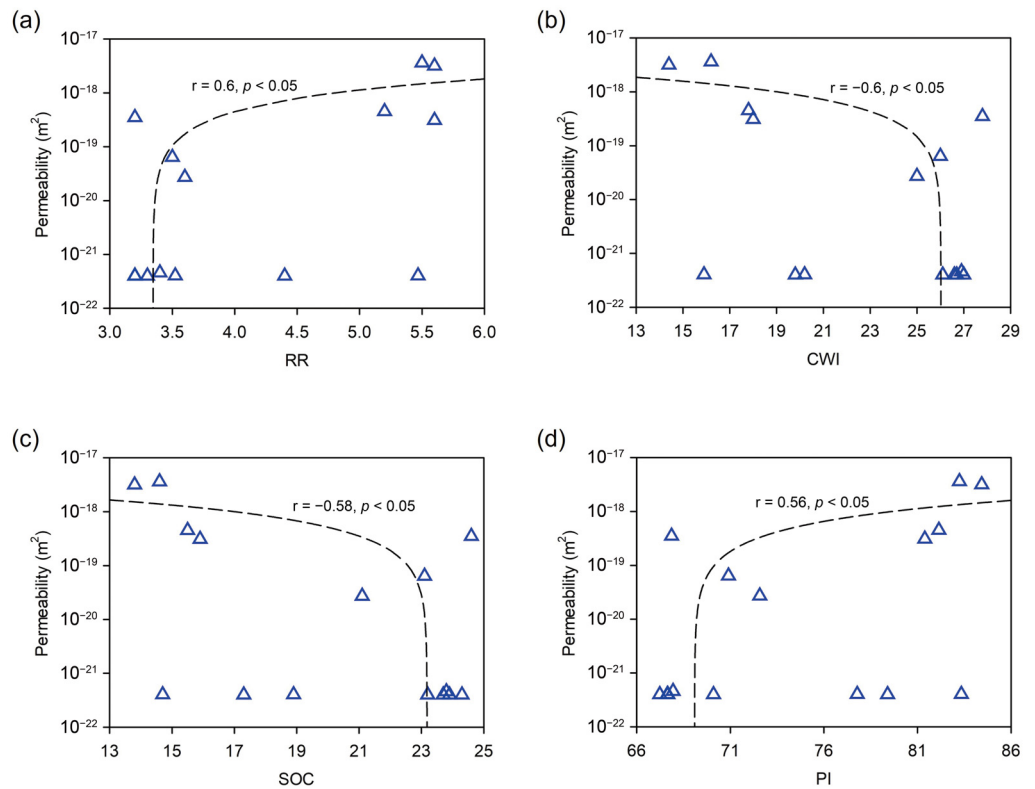


Figure 9. Correlation between permeability and chemical weathering indices ((a) RR; (b) CWI; (c) SOC; (d) PI) for gneiss samples.

The relationship between chemical weathering and permeability in granite has been extensively studied, with many previous works indicating a positive correlation between the degree of chemical weathering and increased permeability [48–52]. This correlation is primarily attributed to the formation of secondary minerals and changes in the pore structure. Studies have shown that as granite undergoes chemical weathering, primary minerals such as feldspars and micas are transformed into secondary minerals like clays and iron oxides. These secondary minerals can occupy pore spaces and create new pathways for fluid movement, thereby increasing the overall permeability of weathered granite [23].

In contrast to these findings, the results of this study suggest a more complex relationship. Although moderate chemical weathering occurred in both rock types, the formation of secondary minerals may have blocked fluid pathways, leading to lower permeability despite increased porosity. Even when rocks have undergone substantial chemical weathering, resulting in increased porosity, permeability can remain low if secondary minerals, such as carbonate and clay, fill the pore spaces and microcracks, obstructing fluid flow [16,37]. This process explains the weak correlation between permeability and the chemical weathering indices observed in this study and highlights the role that secondary mineral formation plays in determining the hydraulic properties of the rock.

The mechanisms observed here, which cause a weak correlation between chemical weathering indices and permeability, are also likely responsible for the weak correlation between chemical weathering indices and V_p in granite samples. Secondary minerals that form as a result of weathering can increase rock density and stiffness, increasing V_p and impacting fluid flow [45,46]. Therefore, in this study, the presence of secondary minerals complicates that relationship, suggesting that the impact of chemical weathering on permeability is strongly influenced by the specific nature of mineral alteration and the infilling of pores.

4.4. Microcrack Effects on Permeability

To investigate the relationship between mineral structure and permeability, samples with varying permeability levels were analyzed using SEM-EDS. Both the granite and gneiss samples were predominantly composed of minerals larger than 100 μm , such as quartz, plagioclase, biotite, and pyroxene (Figure 10). In the high-permeability samples (Figure 10a,c), a greater number of microcracks of various sizes were observed between mineral crystals and the surrounding matrix compared to low-permeability samples (Figure 10b,d). This suggests that the presence and distribution of microcracks significantly contribute to the permeability of crystalline rocks. Microcracks in these rocks typically form along crystal boundaries, within quartz crystals, and along twin planes in plagioclase [16], which further facilitates fluid flow.

In this study, several samples showed low permeability despite having high chemical weathering indices. SEM-EDS analysis demonstrated that the microcracks in these samples were filled with secondary minerals such as calcium carbonate and clay (Figure 11). The infilling of these secondary minerals can obstruct fluid pathways, significantly reducing the overall permeability even in the presence of microcracks [15,30,53]. This suggests that chemical weathering not only increases porosity but also leads to the precipitation of minerals that fill these voids, thereby limiting fluid flow. The dual effect of chemical weathering, creating porosity while simultaneously reducing permeability through mineral infill, explains the observed weak correlation in granite to moderate correlation in gneiss between chemical weathering indices and permeability.

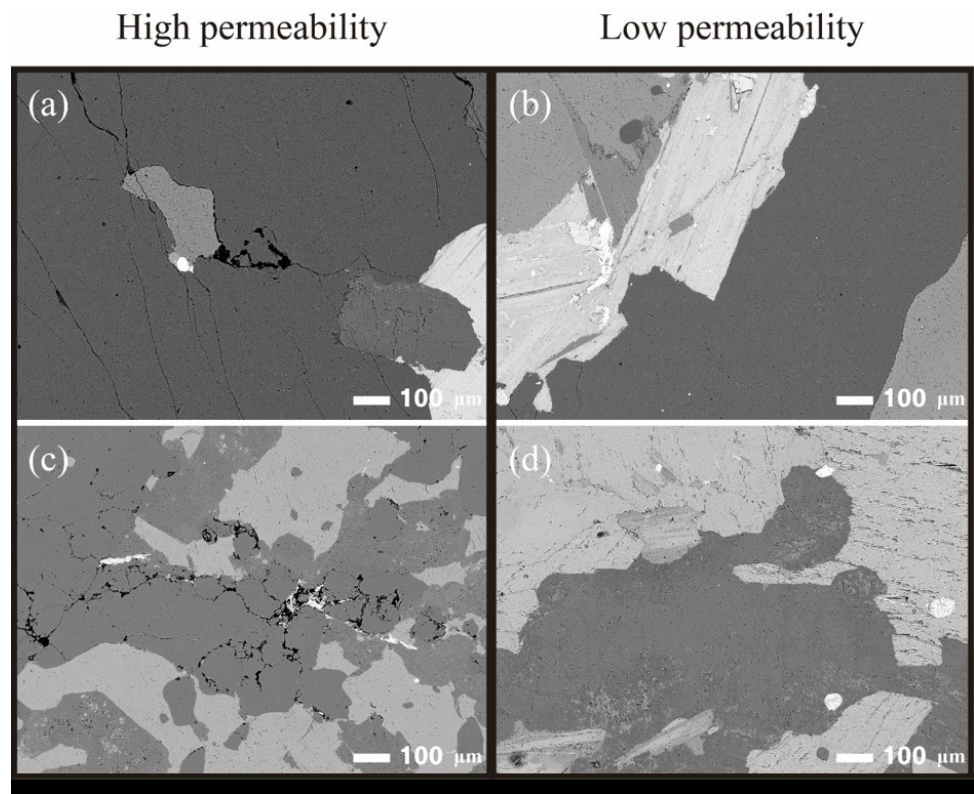


Figure 10. Thin section BSE images for granite and gneiss samples using SEM-EDS analysis. (a,c) show the surfaces of high-permeability granite ($3.11 \times 10^{-19} \text{ m}^2$) and gneiss ($3.17 \times 10^{-18} \text{ m}^2$) samples, respectively. (b,d) show the surfaces of low-permeability granite and gneiss samples (both $< 4 \times 10^{-22} \text{ m}^2$).

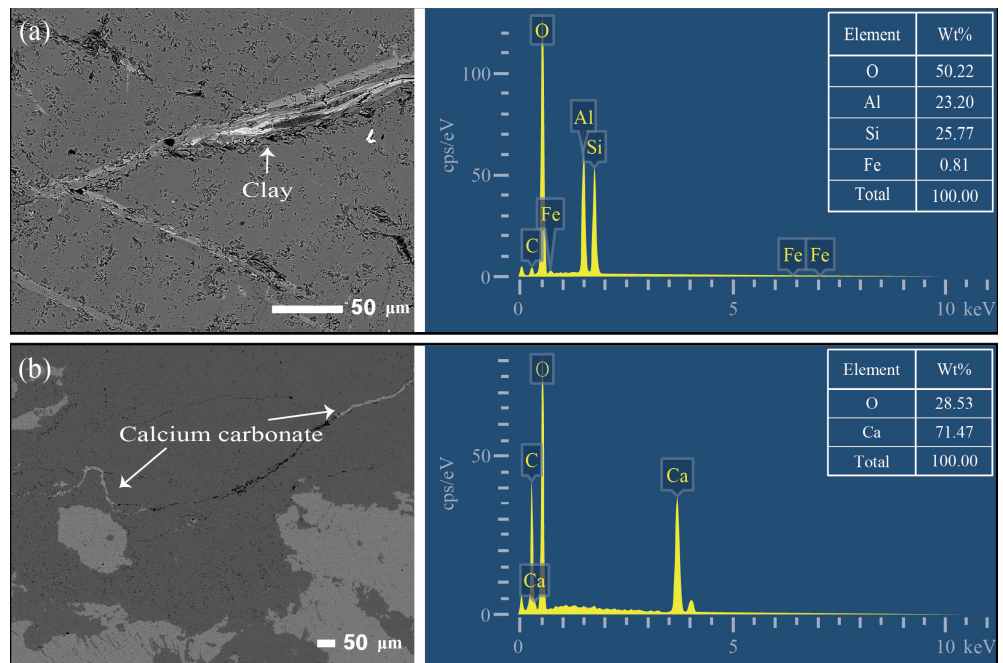


Figure 11. Thin section BSE images and SEM-EDS data for granite and gneiss samples. SEM images show (a) clay filling the cracks in the granite and (b) calcium carbonate filling the cracks in the gneiss.

5. Conclusions

This study investigated the relationships between porosity, permeability, V_p , and chemical weathering indices in granite and gneiss, which are candidate rocks for HLRW disposal sites. The primary goal was to understand the factors influencing the hydrogeological properties of these crystalline rocks. Our results showed a positive correlation between porosity and permeability for both rock types, confirming that higher porosity generally leads to higher permeability. Additionally, V_p results demonstrated that lower rock density is associated with higher permeability.

However, unlike previous studies, we found that many samples showed low permeability despite high chemical weathering indices. SEM-EDS analysis revealed that this discrepancy was due to the presence of secondary minerals, such as clay or carbonate, which formed in the pores and microcracks during chemical weathering. These minerals blocked fluid pathways, thereby reducing permeability even in rocks that had undergone weathering. While extreme chemical weathering often leads to a clear increase in permeability due to the extensive breakdown of the rock structure, in mild to moderate weathering stages, permeability is controlled by a more complex interplay of factors. Specifically, secondary minerals can offset the effects of increased porosity by filling microcracks and voids, impeding fluid flow.

Thus, chemical weathering has a dire effect on permeability. It can either increase permeability through the creation of porosity or decrease it by introducing mineral infill that blocks fluid movement. The findings of this study emphasize the importance of considering not only the degree of weathering but also the presence and connectivity of microcracks, as well as the extent of secondary mineralization, when evaluating the hydrogeological properties of crystalline rocks.

In conclusion, the permeability of crystalline rocks like granite and gneiss is influenced by a combination of porosity, microcrack distribution, and the extent of secondary mineral infill. To accurately assess the hydraulic behavior of these rocks, a comprehensive approach is needed that integrates chemical weathering, microcrack development, and weathering product infillings. These findings are crucial for predicting the hydrogeological behavior of crystalline rocks, especially in applications such as HLRW disposal site selection, rock mechanics, and other geological engineering contexts.

Author Contributions: Conceptualization, J.P. and M.Y.; methodology, S.J. (Seongwoo Jeong) and S.J. (Seonggan Jang); validation, J.P., S.J. (Seongwoo Jeong) and S.J. (Seonggan Jang); formal analysis, S.J. (Seongwoo Jeong) and S.J. (Seonggan Jang); resources, S.J. (Seonggan Jang) and K.K.; data curation, S.J. (Seongwoo Jeong), S.J. (Seonggan Jang) and J.L.; writing—original draft preparation, J.P.; writing—review and editing, K.K. and M.Y.; visualization, J.P., S.J. (Seongwoo Jeong), S.J. (Seonggan Jang) and J.L.; supervision, K.K. and M.Y.; project administration, K.K. All authors have read and agreed to the published version of the manuscript.

Funding: This research received no external funding.

Data Availability Statement: The data presented in this study are available on request from the corresponding author.

Acknowledgments: This work was supported by the Pukyong National University Industry–University Cooperation Research Fund in 2023 (202311970001), Basic Research Project grants (GP2021-004; Integrated management and harm assessment of potentially hazardous elements from geological bedrock in Korea) from the Korea Institute of Geoscience and Mineral Resources (KIGAM), and Global—Learning and Academic research institution for Master’s, PhD students, and Postdocs (LAMP) Program of the National Research Foundation of Korea (NRF) grant funded by the Ministry of Education (No. RS-2023-00301702).

Conflicts of Interest: Jinyoung Park was employed by Wible corporation. The remaining authors declare that the research was conducted in the absence of any commercial or financial relationships that could be construed as a potential conflict of interest.

References

1. Zharikov, A.V.; Velichkin, V.I.; Malkovsky, V.I.; Shmonov, V.M. Experimental Study of Crystalline-Rock Permeability: Implications for Underground Radioactive Waste Disposal. *Water Resour.* **2014**, *41*, 881–895. [\[CrossRef\]](#)
2. Chen, S.; Yang, C.; Wang, G. Evolution of Thermal Damage and Permeability of Beishan Granite. *Appl. Therm. Eng.* **2017**, *110*, 1533–1542. [\[CrossRef\]](#)
3. Konečný, P.; Kožušniková, A. Characterizing Gas Permeability and Pore Properties of Czech Granitic Rocks. *Acta Geodyn. Geomater.* **2016**, *13*, 331–338. [\[CrossRef\]](#)
4. Zhang, W.; Sun, Q.; Zhang, Y.; Xue, L.; Kong, F. Porosity and Wave Velocity Evolution of Granite after High-Temperature Treatment: A Review. *Environ. Earth. Sci.* **2018**, *77*, 1–13. [\[CrossRef\]](#)
5. Montoto San Miguel, M. Characterization of Water Pathways in Low Permeable Rocks at the Rock Matrix Scale: Methodological Review. *J. Iber. Geol.* **2006**, *32*, 197–214.
6. Tsang, C.F.; Neretnieks, I.; Tsang, Y. Hydrologic Issues Associated with Nuclear Waste Repositories. *Water Resour. Res.* **2015**, *51*, 6923–6972. [\[CrossRef\]](#)
7. Cao, X.; Hu, L.; Wang, J.; Wang, J. Regional Groundwater Flow Assessment in a Prospective High-Level Radioactive Waste Repository of China. *Water* **2017**, *9*, 551. [\[CrossRef\]](#)
8. Chen, Y.; Hu, S.; Wei, K.; Hu, R.; Zhou, C.; Jing, L. Experimental Characterization and Micromechanical Modeling of Damage-Induced Permeability Variation in Beishan Granite. *Int. J. Rock Mech. Min. Sci.* **2014**, *71*, 64–76. [\[CrossRef\]](#)
9. Delage, P. On the Thermal Impact on the Excavation Damaged Zone around Deep Radioactive Waste Disposal. *J. Rock Mech. Geotech. Eng.* **2013**, *5*, 179–190. [\[CrossRef\]](#)
10. Liu, L.; Xu, W.Y.; Wang, H.L.; Wang, W.; Wang, R.B. Permeability Evolution of Granite Gneiss During Triaxial Creep Tests. *Rock Mech. Rock Eng.* **2016**, *49*, 3455–3462. [\[CrossRef\]](#)
11. Yasuhara, H.; Kinoshita, N.; Ogata, S.; Cheon, D.S.; Kishida, K. Coupled Thermo-Hydro-Mechanical-Chemical Modeling by Incorporating Pressure Solution for Estimating the Evolution of Rock Permeability. *Int. J. Rock Mech. Min. Sci.* **2016**, *86*, 104–114. [\[CrossRef\]](#)
12. Li, Q.; Wang, Y.; Wang, Y.; San, J.; Li, Q.; Foster, G. Synthetic Process on Hydroxyl-Containing Polydimethylsiloxane as a Thickener in CO₂ Fracturing and Thickening Performance Test. *Energy Sources Part A Recovery Util. Environ. Eff.* **2018**, *40*, 1137–1143. [\[CrossRef\]](#)
13. Li, Q.; Han, Y.; Liu, X.; Ansari, U.; Cheng, Y.; Yan, C. Hydrate as a By-Product in CO₂ Leakage during the Long-Term Sub-Seabed Sequestration and Its Role in Preventing Further Leakage. *Environ. Sci. Pollut. Res.* **2022**, *29*, 77737–77754. [\[CrossRef\]](#) [\[PubMed\]](#)
14. Billiotte, J.; Yang, D.; Su, K. Experimental Study on Gas Permeability of Mudstones. *Phys. Chem. Earth* **2008**, *33*, S231–S236. [\[CrossRef\]](#)
15. Xie, M.; Mayer, K.U.; Claret, F.; Alt-Epping, P.; Jacques, D.; Steefel, C.; Chiaberge, C.; Simunek, J. Implementation and Evaluation of Permeability-Porosity and Tortuosity-Porosity Relationships Linked to Mineral Dissolution-Precipitation. *Comput. Geosci.* **2015**, *19*, 655–671. [\[CrossRef\]](#)
16. Kubo, T.; Matsuda, N.; Kashiwaya, K.; Koike, K.; Ishibashi, M.; Tsuruta, T.; Matsuo, T.; Sasao, E.; Lanyon, G.W. Characterizing the Permeability of Drillhole Core Samples of Toki Granite, Central Japan to Identify Factors Influencing Rock-Matrix Permeability. *Eng. Geol.* **2019**, *259*, 105163. [\[CrossRef\]](#)
17. Nara, Y.; Meredith, P.G.; Yoneda, T.; Kaneko, K. Influence of Macro-Fractures and Micro-Fractures on Permeability and Elastic Wave Velocities in Basalt at Elevated Pressure. *Tectonophysics* **2011**, *503*, 52–59. [\[CrossRef\]](#)
18. Wang, H.; Pan, J.; Wang, S.; Zhu, H. Relationship between Macro-Fracture Density, P-Wave Velocity, and Permeability of Coal. *J. Appl. Geophys.* **2015**, *117*, 111–117. [\[CrossRef\]](#)
19. Gupta, A.S.; Rao, S.K. Weathering Indices and Their Applicability for Crystalline Rocks. *Bull. Eng. Geol. Environ.* **2001**, *60*, 201–221. [\[CrossRef\]](#)
20. Sharma, A.; Rajamani, V. Major Element, REE, and Other Trace Element Behavior in Amphibolite Weathering under Semi-arid Conditions in Southern India. *J. Geol.* **2000**, *108*, 487–496. [\[CrossRef\]](#)
21. Ban, J.-D.; Moon, S.-W.; Lee, S.-W.; Lee, J.-G.; Seo, Y.-S. Physical and Chemical Weathering Indices for Biotite Granite and Granitic Weathered Soil in Gyeongju. *J. Eng. Geol.* **2017**, *27*, 451–462. [\[CrossRef\]](#)
22. Jayawardena, U.d.S.; Izawa, E. A New Chemical Index of Weathering for Metamorphic Silicate Rocks in Tropical Regions: A Study from Sri Lanka. *Eng. Geol.* **1994**, *36*, 303–310. [\[CrossRef\]](#)
23. Lee, S.H.; Chung, C.K.; Song, Y.W.; Woo, S.I. Relationship between Chemical Weathering Indices and Shear Strength of Highly and Completely Weathered Granite in South Korea. *Appl. Sci.* **2021**, *11*, 911. [\[CrossRef\]](#)
24. Tijani, M.N.; Okunlola, O.A.; Abimbola, A.F. Lithogenic Concentrations of Trace Metals in Soils and Saprolites over Crystalline Basement Rocks: A Case Study from SW Nigeria. *J. Afr. Earth Sci.* **2006**, *46*, 427–438. [\[CrossRef\]](#)
25. Talabi, A.O. Weathering of Meta-Igneous Rocks in Parts of the Basement Terrain of Southwestern Nigeria: Implications on Groundwater Occurrence. *Int. J. Sci. Res. Publ.* **2014**, *5*, 1–17.
26. Udagedara, D.T.; Oguchi, C.T.; Gunatilake, A.A.J.K. Combination of Chemical Indices and Physical Properties in the Assessment of Weathering Grades of Sillimanite-Garnet Gneiss in Tropical Environment. *Bull. Eng. Geol. Environ.* **2017**, *76*, 145–157. [\[CrossRef\]](#)
27. Chiu, C.F.; Ng, C.W.W. Relationships between Chemical Weathering Indices and Physical and Mechanical Properties of Decomposed Granite. *Eng. Geol.* **2014**, *179*, 76–89. [\[CrossRef\]](#)

28. Dwivedi, R.D.; Goel, R.K.; Prasad, V.V.R.; Sinha, A. Thermo-Mechanical Properties of Indian and Other Granites. *Int. J. Rock Mech. Min. Sci.* **2008**, *45*, 303–315. [[CrossRef](#)]
29. Liu, X.; Zhang, X.; Kong, L.; Wang, G.; Liu, H. Chemical Weathering Indices and How They Relate to the Mechanical Parameters of Granite Regolith from Southern China. *Catena* **2022**, *216*, 106400. [[CrossRef](#)]
30. Sausse, J.; Jacquot, E.; Fritz, B.; Leroy, J.; Lespinasse, M. Evolution of Crack Permeability during Fluid–Rock Interaction. Example of the Brézouard Granite (Vosges, France). *Tectonophysics* **2001**, *336*, 199–214. [[CrossRef](#)]
31. Choi, J. Comparative Analysis of the Joint Properties of Granite and Granitic Gneiss by Depth. *Econ. Environ. Geol.* **2019**, *52*, 189–197. [[CrossRef](#)]
32. Jo, H.J.; Cheong, A.C.S.; Yi, K.; Li, X.H. Juxtaposition of Allochthonous Terranes in the Central Korean Peninsula: Evidence from Zircon U–Pb Ages and O–Hf Isotopes in Jurassic Granitoids. *Chem. Geol.* **2018**, *484*, 136–147. [[CrossRef](#)]
33. Somerton, W.H.; Söylemezoglu, I.M.; Dudley, R.C. Effect of Stress on Permeability of Coal. *Int. J. Rock Mech. Min. Sci. Geomech. Abstr.* **1975**, *12*, 129–145. [[CrossRef](#)]
34. Klinkenberg, L.J. The Permeability of Porous Media to Liquids and Gases. In Proceedings of the Drilling and Production Practice, New York, NY, USA, 1 January 1941; pp. 200–213.
35. Chittleborough, D.J. Indices of Weathering for Soils and Palaeosols Formed on Silicate Rocks. *Aust. J. Earth Sci.* **1991**, *38*, 115–120. [[CrossRef](#)]
36. Ruxton, B.P. Measures of the Degree of Chemical Weathering of Rocks. *J. Geol.* **1968**, *76*, 518–527. [[CrossRef](#)]
37. Irfan, T.Y. Mineralogy, Fabric Properties and Classification of Weathered Granites in Hong Kong. *Q. J. Eng. Geol. Hydrogeol.* **1996**, *29*, 5–35. [[CrossRef](#)]
38. Sueoka, T. Identification and Classification of Granitic Residual Soils Using Chemical Weathering Index. In Proceedings of the International Conference on Geomechanics in Tropical Soils, Singapore, 12–14 December 1988; Volume 2, pp. 55–61.
39. Okewale, I.A. Applicability of Chemical Indices to Characterize Weathering Degrees in Decomposed Volcanic Rocks. *Catena* **2020**, *189*, 104475. [[CrossRef](#)]
40. Reiche, P. Graphic Representation of Chemical Weathering. *J. Sediment. Res.* **1943**, *13*, 58–68. [[CrossRef](#)]
41. Brace, W.F. Permeability of Crystalline and Argillaceous Rocks. *Int. J. Rock Mech. Min. Sci. Geomech.* **1980**, *17*, 241–251. [[CrossRef](#)]
42. David, C.; Menéndez, B.; Darot, M. Influence of Stress-Induced and Thermal Cracking on Physical Properties and Microstructure of La Peyratte Granite. *Int. J. Rock Mech. Min. Sci.* **1999**, *36*, 433–448. [[CrossRef](#)]
43. Wang, H.; Xu, W.; Shao, J.; Skoczylas, F. The Gas Permeability Properties of Low-Permeability Rock in the Process of Triaxial Compression Test. *Mater. Lett.* **2014**, *116*, 386–388. [[CrossRef](#)]
44. Medina, C.R.; Rupp, J.A.; Barnes, D.A. Effects of Reduction in Porosity and Permeability with Depth on Storage Capacity and Injectivity in Deep Saline Aquifers: A Case Study from the Mount Simon Sandstone Aquifer. *Int. J. Greenh. Gas Control.* **2011**, *5*, 146–156. [[CrossRef](#)]
45. Mavko, G.; Mukerji, T.; Dvorkin, J. *The Rock Physics Handbook: Tools for Seismic Analysis in Porous Media*; Cambridge University Press: Cambridge, England, 1998.
46. Schön, J.H. *Physical Properties of Rocks: Fundamentals and Principles of Petrophysics*, 2nd ed.; Elsevier Science: Amsterdam, The Netherlands, 2015.
47. Wyllie, M.R.J.; Gregory, A.R.; Gardner, G.H.F. An experimental investigation of factors affecting elastic wave velocities in porous media. *Geophysics* **1958**, *23*, 459–493. [[CrossRef](#)]
48. Briški, M.; Stroj, A.; Kosović, I.; Borović, S. Characterization of Aquifers in Metamorphic Rocks by Combined Use of Electrical Resistivity Tomography and Monitoring of Spring Hydrodynamics. *Geosciences* **2020**, *10*, 137. [[CrossRef](#)]
49. Gu, X.; Remppe, D.M.; Dietrich, W.E.; West, A.J.; Lin, T.C.; Jin, L.; Brantley, S.L. Chemical Reactions, Porosity, and Microfracturing in Shale during Weathering: The Effect of Erosion Rate. *Geochim. Cosmochim. Acta* **2020**, *269*, 63–100. [[CrossRef](#)]
50. Dearman, W.R.; Baynes, F.J.; Irfan, T.Y. Engineering Grading of Weathered Granite. *Eng. Geol.* **1978**, *12*, 345–374. [[CrossRef](#)]
51. Kim, S.; Park, H.D. The Relationship between Physical and Chemical Weathering Indices of Granites around Seoul, Korea. *Bull. Eng. Geol. Environ.* **2003**, *62*, 207–212. [[CrossRef](#)]
52. Worthington, S.R.H.; Davies, G.J.; Alexander, E.C. Enhancement of Bedrock Permeability by Weathering. *Earth. Sci. Rev.* **2016**, *160*, 188–202. [[CrossRef](#)]
53. Nishimoto, S.; Yoshida, H. Hydrothermal Alteration of Deep Fractured Granite: Effects of Dissolution and Precipitation. *Lithos* **2010**, *115*, 153–162. [[CrossRef](#)]

Disclaimer/Publisher’s Note: The statements, opinions and data contained in all publications are solely those of the individual author(s) and contributor(s) and not of MDPI and/or the editor(s). MDPI and/or the editor(s) disclaim responsibility for any injury to people or property resulting from any ideas, methods, instructions or products referred to in the content.